Hydrogeology of glaciated continental margins (Storfjorden, S Svalbard, Norway): Constraints from permeability and consolidation experiments.

Màster en Ciències del Mar: Oceanografia i Gestió del Medi Marí

Jaume Llopart Serra

September 2011

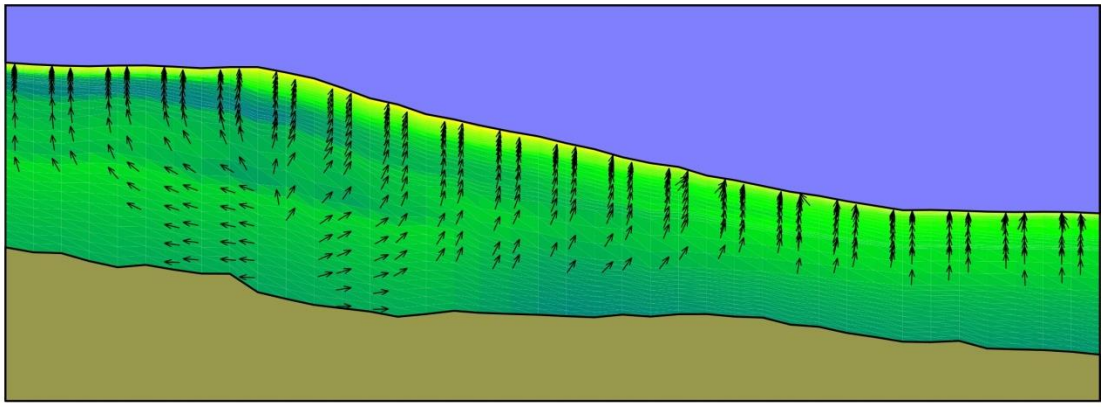

Director: Dr. Roger Urgeles Esclasans, Dpt. Geologia Marina, Institut de Ciències del Mar (CSIC).

Co-director: Dr. Angelo Camerlenghi, Dpt. d'Estratigrafia, Paleontologia i Geociències Marines, Facultat de Geologia, Universitat de Barcelona.

INDEX

1. Abstract

Climate variations induce important stress changes in seafloor and sub-seafloor sediments of Polar Regions that can result in massive catastrophic slope failure events. These climate variations control glacial advances and retreats, which (a) cause significant load changes in the sedimentary column and redistribution of interstitial fluids and (b) induce a particular margin stratigraphic pattern and permeability architecture. A series of laboratory tests have been carried out to understand the compressibility and permeability characteristics of sediments from polar margins, and how burial affects these properties that control interstitial fluid flow and pore pressure build-up. The results are used together with margin stratigraphic models obtained from seismic reflection data, in basin analysis numerical models to understand focusing of fluids in glaciated continental margins and influence on timing and location of slope instabilities.

The samples tested have shown that turbidites have higher initial hydraulic conductivity (1.2×10^{-7} m/s compared to 5.9×10^{-10} m/s) and compressibility (0.35 versus 0.19 than glacial debris flows. Both of these physical properties decrease with burial depth... Modelling shows that low porosities and hydraulic conductivities develop on the upper Quaternary sediments of the continental shelf and shelf break compared to the lower stratigraphic levels of the margin and lower continental slope and rise. The higher sedimentation rates around the shelf break due to progradation are responsible for fluid flow divergence, which affects the entire fluid flow pattern of the continental margin. In response to this, overpressure and low effective stresses develop at the outer continental shelf and the shelf break between 550-1500 mbsf indicating a likely pre-conditioning for deep-seated failure.

2. Introduction

2.1. General Context

During the last decades large submarine landslides have been widely discovered in Polar Regions. The Norwegian margin has been subject of a comprehensive study motivated by the occurrence of gas and oil fields associated to nearby landslides. Large and medium-size landslides are well documented (i.e. the Trænadjupet Slide and the Andøya Slide, Bjørnøyrenna Slide and the Isfjorden Slide), including the largest known submarine landslide; the Storegga Slide with a volume of 5600 km^3 *(Bugge et al., 1988)*. The thick deposits accumulated during glacial and interglacial cycles have been subject to ice sheets dynamics, loading and unloading by the grounded ice sheet, glacio-eustatic sea-level variations, glacio-isostatic rebound and associated seismicity, etc *(Bugge et al., 1987; Mulder and Moran, 1995)*. Under these constraints, sediment interstitial fluids must have played a significant role in continental margin development, resulting in sediment instability when combined with depositional over steeping (Dimakis et al., 2000*)*. Development of excess pore pressure from non-equilibrium consolidation, as well as from methane hydrates dissociation and dissolution (Sultan et al., 2004), represent a geohazard because they are one of the major controls on submarine slope failure initiation (Vorren et al., 1998).

2.2. Scientific Problem

The Barents Sea region has been affected by several glacial and interglacial cycles during the Plio-Pleistocene. During ice advance maxima, the ice thickness was variable but some authors estimate values ranging from 1 to 3 km *(Elverhøi et al., 1993)*. The different cycles of continental margin loading and unloading by ice and the spatial variability in its thickness across the Barents Sea continental margin probably caused significant changes in fluid flow circulation patterns. Furthermore, ice sheets and particularly ice streams

provide a large amount of sediments to the shelf edge and slope during glaciations. In the western Barents Sea continental margin (i.e. Storfjorden Fan, Fig.1; Bear Island Fan) large volumes of glacial sediments deposited at high sedimentation rates of 0.25 to 0.62 m/kyr, with recorded maxima of 1.96 m/kyr (Hjelstuen et al., 1996) and 3.75 m/kyr (Pedrosa et al., 2011).. Climatically modulated sedimentation in polar margins (Fig. 2) creates large heterogeneities in sediment type and provides large spatial variability in physical properties of marine sediments (Fig .3). How this affects the continental margin hydrogeology and fluid flow pattern is not well known yet.

The aims of this study is therefore to: 1) characterize the compression and permeability characteristics of glacial-deglacial-interglacial marine sediments of a polar continental margin and 2) to reconstruct the paleohydrogeological evolution and determine how continental margin architecture and physical properties couple to control fluid flow patterns.

2.3. Geologic framework

The Barents Sea is enclosed on its western and northern boundary by a passive continental margin (Engen et al., 2008). The continental shelf edge on its western boundary extends from about 70ºN to 80ºN and roughly strikes in the N-S direction. The continental shelf is incised by several glacial troughs, which broadly trend ENE-WSW (e.g. the Storfjorden Trough and the Bear Island Trough). At the mouths of these troughs, large convex depositional bodies develop, which correspond to fans mainly made of glacial sediments. The dimensions of these fans are proportional to their troughs and drainage area *(Vorren, et al., 1998).* The largest fan in this area is the Bear Island Trough Mouth Fan (TMF) with around $4 \cdot 10^5$ km^3 of sediments (Elverhøi et al., 1998). The oceanic basement of the Western Barents Sea is of Eocene-Miocene age. The basement is overlain by a prominent Plio-Pleistocene prograding wedge, which resulted from a significant increase in the sediment input from the

margins of the Barents Sea. This induced a seaward migration of the shelf break of up to 150 km in places *(Dahlgren et al., 2005)*. *Butt et al. (2002)* inferred using numerical modelling techniques that the continental margin of the western Barents Sea had subaerial conditions in the earliest Late Pliocene. Despite, the onset of the main Northern Hemisphere Glaciations on the Barents/Svalbard margin is considered to have occurred at about 2.6 Ma (Butt et al., 2000), terrigenous sediments were initially of fluvial and glacio-fluvial source (Forsberg et al., 1999; Dahlgren et al., 2005). From the Middle Pleistocene onwards, they were originated from subglacial sediment discharge from ice streams grounded at the shelf edge to form TMFs. Faleide et al. (1996) established three main sequences (GI–GIII) and identified seven regional seismic reflectors (R7–R1) along the western margin (Fig. 4). R7 marks the onset of glacially-dominated deposition along the margin when glaciers reached the shelf break off Svalbard and the Storfjorden Trough, while expansion to the shelf break in the southwestern Barents Sea was delayed until R5 time along the margin. “R” reflectors marks a change in erosion-accumulation dynamics also a change in reflection patterns.

With respect to sediment types, the Barents/Svalbard margin can be divided in three zones: the continental shelf, the self-edge and upper/middle slope and the lower slope and abyssal plain. The first one is mainly composed of basal tills and grounding zone wedges. The second is made of till deltas that were brought to the grounding-line and interbeded with ice rafted detritus (IRD), debris flows, hemipelagic sediments and turbidity currents mainly resulting from dense subglacial melt water. This alternation was controlled by advance and retreat of ice sheets and the amount of sediment transported subglacially to the shelf edge during glacial maxima. The lower slope and proximal abyssal plain are made of distal turbidity currents, hemipelagic sediments, contourites and IRD. Fig 1 shows a schematic picture of the shelf edge and the upper/middle slope processes.

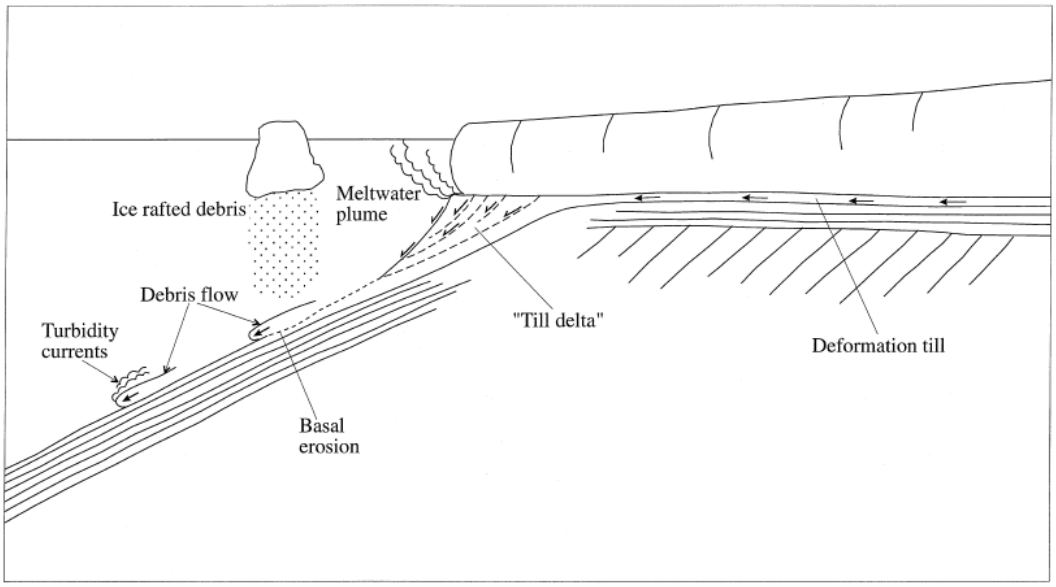

Fig 1 Schematic model showing the main sedimentary processes on the shelf break and upper slope during the presence of an ice sheet at the shelf break (from Laberg and Vorren, 1995).

The study area (Fig 2) is located in the Storfjorden Trough Mouth Fan (TMF) south of the Svalbard archipelago. This fan covers an area of about 40.000 km^2 and has a radius of about 190 km, developed concentrically off the Storfjorden trough. The upper and middle fan gradients along the central fan axis are 1.8° and 1.0°, respectively, while the lower fan gradient is about 0.2° or less *(Laberg and Vorren, 1996).*

3. Methods

Data acquisition

The samples used for laboratory testing in this study were acquired between July 4-15, 2007 in the frame of the project “SVAIS - The development of an Arctic ice stream-dominated sedimentary system: The southern Svalbard continental margin”. Five piston cores between 5-10 m pipe length and a gravity core with a 3 m long barrel (SVAIS-06) were collected (Fig. 2). Samples from the SVAIS-02 core (Fig. 3) have been used for geotechnical testing, specifically the intervals 1.4-1.5 m depth (SVAIS-02-02), 3.4-3.5 m depth (SVAIS-02-04) and 5.4-6.4 m depth (SVAIS-02-06).

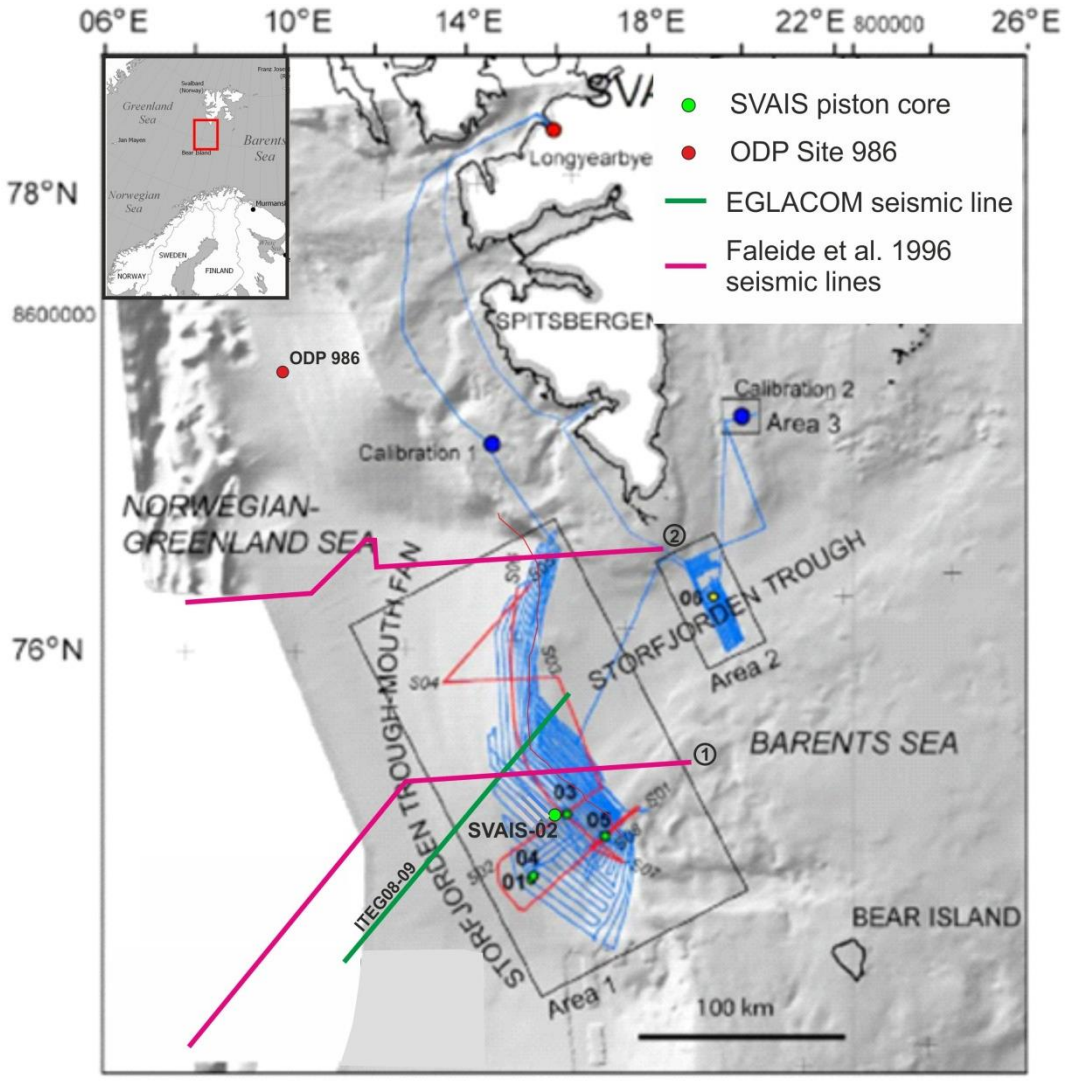

Fig 2 Location of the study area. Modified from SVAIS Cruise Report 2007.

The stratigraphy and 2D architecture of the different units used to perform the hydrogeological modelling correspond to the seismic units defined in between reflectors R1-R7 described in Faleide et al., 1996. These reflectors were picked on seismic line ITEG08-09 acquired during the Italian cruise EGLACOM (Fig. 4) led by the Istituto Nazionale di Oceanografia e di Geofisica Sperimentale (Italy) in July 2008. The R7 and the OB (top of Oceanic Basement) reflectors correspond with the projected position of these reflectors on line ITEG08-09 made from the two seismic lines north and south of Storfjorden included in Faleide et al. (1996) as the line ITEG08-09 did not have enough penetration to image these reflectors. The velocities for the time to depth conversion have been approximated from Butt et al., 2000.

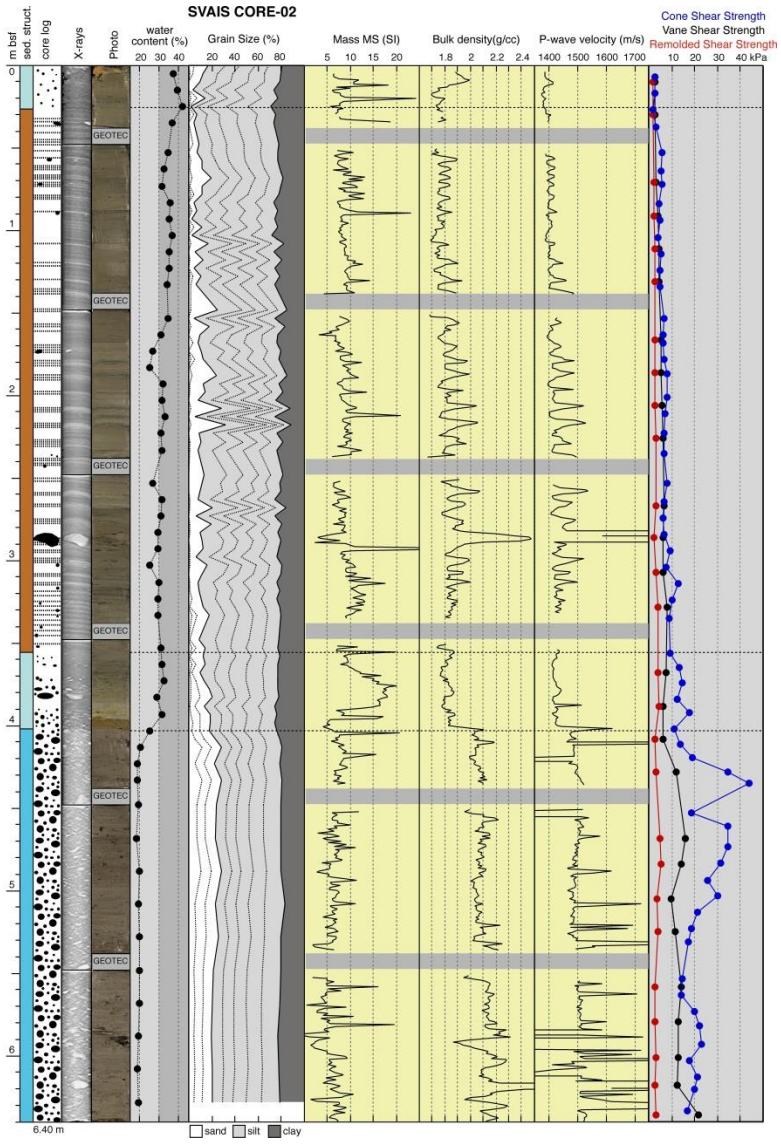

Fig. 3 Core SVAIS-02 description and core logging analysis. From left to right logs show intervals in relation to glaciation history, sedimentary facies, X-Ray image, core photos.

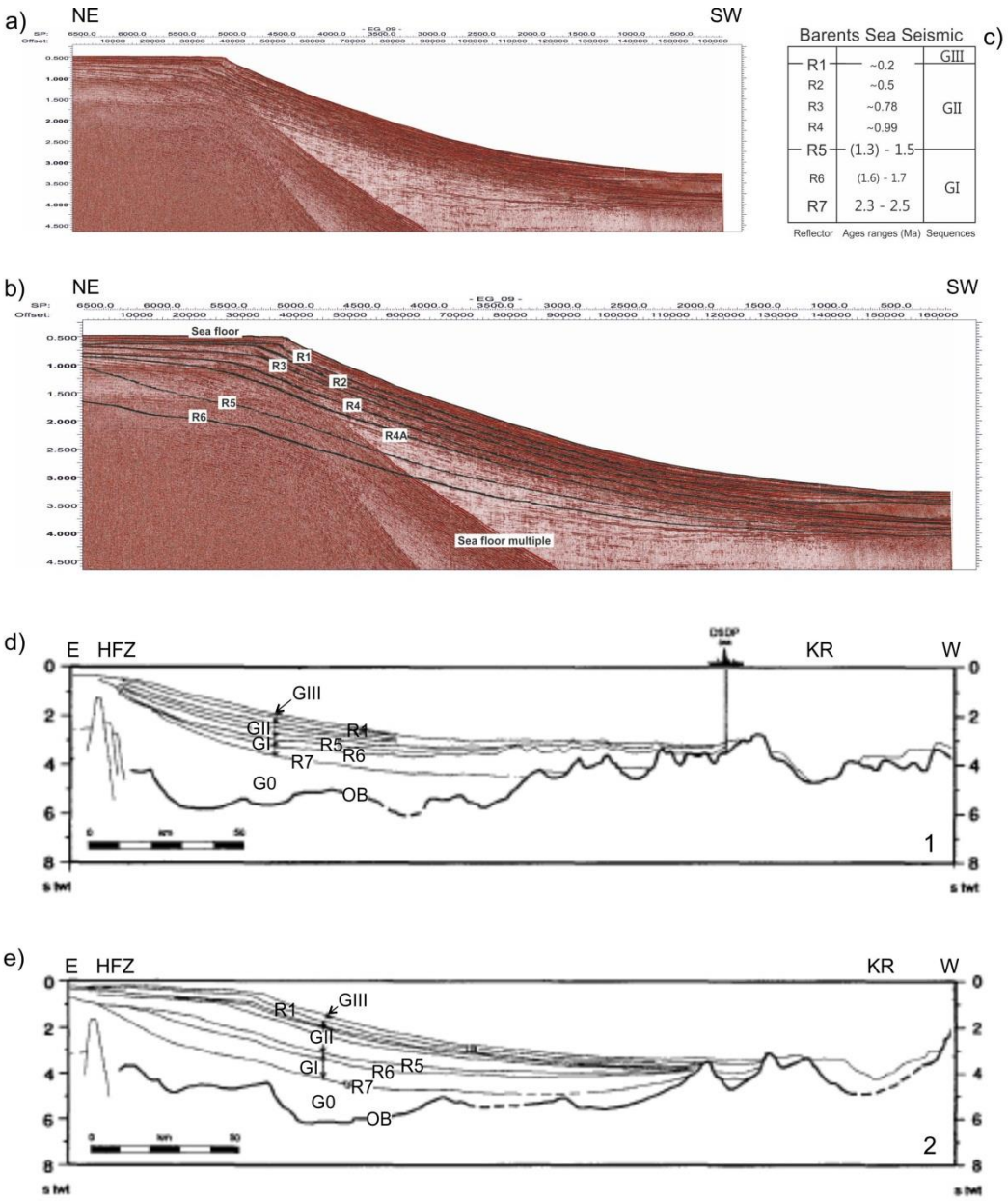

Fig. 4 a) uninterpreted and b) interpreted EGLACOM ITEG08-09 seismic line used for "BASIN" modelling. c) age ranges for seismic reflectors (Hjelstuen et al., 2007). d), e) seismic lines from Faleide et al. 1996.

Testing procedures: Consolidation Test

To accomplish the set of objectives described above consolidation and permeability tests were performed using a GDS Rowe & Barden-type Consolidation cell equipped with three 2MPa advanced pressure/volume controllers (Fig. 5) (Table 1) to control respectively: upper chamber pressure, back pressure and base pressure. The upper chamber allows to apply a vertical stress directly on the sample. This stress is transmitted to the sample with the

aid of a top bag that separates the upper chamber from the sediment specimen. The back pressure is transmitted directly to the top of the specimen through a porous stone. The base pressure is connected to the bottom of the specimen through a second porous stone. Establishing a hydraulic gradient between the base pressure and back pressure controllers allows to determine the permeability at a given consolidation stress. In addition the cell is equipped with an axial displacement and pore pressure transducers to measure settlement and pore pressure at the base of the sample.

Moreover, for the three selected samples, Atterberg Limits were also determined. The liquid limit was determined using an 80g, 60º apex Swedish Fall cone device, while the plastic limit was estimated from the rolled thread of sediment method *(Karlsson, R., 1961)*. All tests have been carried out using the "British Standard Methods of test for Soils for civil engineering purposes" BS1377 *(BSI Standards, 1990)*. Consolidation proceeded in three phases:

- **Saturation**: to guarantee that all the applied stresses in the subsequent consolidation phase are applied to the soil. The upper chamber pressure and back pressure are increased at equal pressure increments so that the total stress increases while the effective stress remains constant, thus bringing air into solution.

- **Consolidation**: Consolidation stress is applied to the sample in steps by increasing the upper chamber pressure and allowing the sample to freely drain. The total stress level can be selected and applied instantly while the pore pressure dissipates. For practical purposes the maximum time allowed for dissipation was 24 hours, but pore pressure fully dissipated before this period was reached. Each test involved several loading and unloading stages corresponding to different effective stress conditions. The condition that had to be met for moving from one stage to another was that the pore pressure resulting from an upper chamber load increment had dissipated completely, implying that, at least the primary consolidation was finished. Fig. 6 shows pore pressure dissipation and the sample strain during every load stage. The consolidation test also allows to determine the pre-consolidation pressure by plotting the final deformation after primary consolidation for all consolidation stresses. This curve can be divided in three portions: at low effective stresses

the curve displays a low deformation gradient resulting from sample recompression to field stresses. The second part is the steepest one, and represents the virgin consolidation line. The third part is similar in slope to the first one and results from unloading and elastic recovery. The passage from recompression to the virgin consolidation line occurs near the pre-consolidation pressure, the maximum stress that the sample has been subject to in the past. To determine the pre-consolidation pressure the graphic method of Casagrande (1936) has been used. This method consists in 1. Drawing a horizontal line from the point of maximum curvature on the consolidation curve, 2. drawing a line tangent to the curve at that point, 3. bisecting the angle made from the horizontal and tangent lines, and 4. extend the "straight portion" of the recompression curve (low effective stress, high void ratio: horizontal on the left of the graph) up to the bisector line. The point where the lines in 3 and 4 dissect is the pre-consolidation pressure.

	Sample (H x Diam)	Maximum Pressure	Pressure resolution	Volume resolution
R&B Cell ADVCTS (Controller)	20 x 50 mm	2 Mpa	0.5 kPa	0.5 mm^3

Table 1 Rowe and Barden Cell sample dimensions and controller properties.

Fig. 5 Rowe and Barden Cell and pressure/volume controllers.

Sample deformation is measured as strain. To convert from strain to void ratio (Fig. 7) the following formulation was used:

$$V_s = V_i - \left(\frac{\left(M^i - M_d^i\right)}{(1-S)\cdot\rho_w}\right)\cdot 1000 \quad (1) \qquad h_s = \frac{V_s}{A} \quad (2) \qquad e = \frac{h^i - h_s}{h_s} \quad (3)$$

Where:

V_s: volume of solidus ($mm^{3)}$;

V_i: initial volume of specimen (mm^3);

S: salinity (%);

ρ_w: water density ((998.2071 kg/m^3));

A: area of specimen (mm^2);

h^i: initial height of specimen (mm);

M^i: initial mass of specimen (g);

$M^d{}_i$: initial dry mass of specimen (g);

H_s: equivalent height of solidus (mm);

Another parameter derived from the consolidation test data is the specific storage. This parameter is a sediment physical property that characterizes the capacity of an aquifer to release groundwater from storage in response to a decline in hydraulic head (Fig. 8).

-**Permeability**: After each consolidation step permeability measurement was carried out creating a pressure gradient between both sides of the specimen and measuring the water volume that circulated through it in a given time interval. Darcy's law was then used to determine the sample permeability. In addition to this flow-through permeability test performed at the end of each loading stage, permeability can also be derived from the consolidation test itself using the following formulation :

$$Q = K \cdot A \cdot \frac{\Delta h}{L} \quad (4) \qquad \mathrm{k} = K\frac{\mu}{\rho g} \quad (5)$$

$$\mathrm{m_v} = \frac{\Delta H_2 - \Delta H_1}{H_0 - \Delta H_1} \times \frac{1000}{\sigma_2' - \sigma_1'} \quad (6) \qquad \mathrm{H_m} = \frac{(H_i + H_f)^2}{4} \quad (7) \qquad \mathrm{C_v} = \frac{0.197 \cdot H_m^2}{T_{50}} \quad (8)$$

$$\mathrm{K} = \mathrm{C_v} \cdot \mathrm{m_v} \cdot \mathrm{g} \cdot \rho_\mathrm{w} \quad (9)$$

Where:
Q: flow (m3/s);
K: hydraulic conductivity (m/s);
Δh: hydraulic head;
A: sample area;
L: sample length;
ΔH_1: cumulative change in height of the specimen up to the end of the previous consolidation stage (mm);
ΔH_2: cumulative change in height of the specimen up to the end of the consolidation stage being considered (mm);
H_o: initial height of the specimen (mm);
σ_1': effective pressure applied to the specimen for the previous consolidation stage (kPa);
σ_2': effective pressure applied to the specimen for the consolidation stage considered (kPa).

m_v: volume compressibility coefficient during the load increment;
H_m: average thickness of specimen during the load increment (mm);
H_i: Initial thickness of sample at stage (mm);
H_f: Final thickness of sample at stage (mm);
C_v: consolidation index during the load increment;
K: hydraulic conductivity;
μ: dynamic viscosity (0.001002 Pa·s);
ρ: density of the fluid (998.2071 kg/m^3);
g: acceleration of gravity (9.81 m/s^2);

The permeabilities derived from both methods at each stage yield different values and as a result the estimated initial permeability values are also different (Fig 8a). The permeability derived from the consolidation test is based on the volume compressibility index and the consolidation index, whereas, the Darcy's law method is directly based on an objective measurement of the fluid flow through the sample. For this reason, the values derived from Darcy's law method is considered more accurate and will be used in margin hydrogeological modelling.

Hydrogeological Model

Using the Finite Element Software "BASIN" (Bitzer et al., 1996, 1999) continental margin hydrogeological modelling has been carried out to simulate the fluid migration and pore pressure development processes involved in glaciated continental margins. "BASIN" uses finite-element meshes with triangular elements. The program calculates the sedimentary and hydrogeological evolution for a given set of geological initial (Table 2) and boundary conditions. The hydrodynamic evolution is calculated from these initial conditions and subsequent changes of basin geometry are calculated from sedimentation rates, compaction and pore fluid mobilisation amongst others. Sedimentologic and hydraulic parameters are stored at discrete time steps allowing to analyse the temporal evolution of the basin. A maximum of four different sediment types, which may be mixed during sedimentation, can be defined. Compaction and fluid flow are coupled through the consolidation equation and the nonlinear form of the equation of state for porosity, allowing non-equilibrium compaction and overpressure to be calculated. Instead of empirical porosity-effective stress equations, a physical consistent consolidation model is applied which incorporates a porosity dependent sediment compressibility. The output data allow plotting results in a two-dimensional vertical cross section and to create different animated plots like porosity, hydraulic conductivity and pore pressure evolution. In this study pore pressure

is most often described in terms of overpressure (λ), defined as (Urgeles et al., 2010)*:*

$$\lambda = (P - P_h)/(\sigma_v - P_h) \quad (10)$$

where *P* is pore pressure, P_h is the hydrostatic pressure and σ_v is lithostatic or total stress. A value of 0 implies hydrostatic conditions, a value of 1 means pore pressure equals lithostatic stress.

For modelling with “BASIN”, we use initial sediment physical properties measured during consolidation/permeability testing (Table 2): SVAIS-02-02 and SVAIS-02-04 (turbidites) and SVAIS-02-06 (GDF’s), or derived from values reported in the literature: tills (Shaver, 1998, Solheim et al., 1991) and hemipelagic sediments (Butt et al., 2000; Urgeles et al., 2010). For the latter we use mostly sediment parameters from the ODP Site 986C/D from (Butt et al. 2000). The initial thickness (H_i) of different strata used as input for the model was calculated using van Hinte (1978)´s decompaction equation:

$H_i=(1-\phi_f)*H_f/(1-\phi_i)$, (11)

where ϕ_i is the initial porosity, ϕ_f is the present-day porosity and H_f is the present sediment thickness.

4. Results

Consolidation/permeability testing on samples SVAIS-02-02 and SVAIS-02-04 was performed on plumite-turbidite type sediments, while on sample SVAIS-02-06 the test was performed on glacigenic debris flows (GDF's). The core photo, X-Ray, grain size and other analysis on this core (not performed in this study) are shown in Fig 3 for reference (see also Lucchi et al., 2011). Figure 6 shows the pore pressure dissipation and the samples deformation for every stage. While testing sample SVAIS-02-02 a problem leak on the top bag that separates the upper chamber from the sediment specimen occurred and the test had to be stopped. After arranging the problem, the test was recommenced. The results from both parts of the test merge well and the virgin consolidation line displays a similar gradient (fig 7).

Atterberg Limits show that turbidites have higher plastic and liquid limits than GDF's (see Table 2). Pre-consolidation pressures for the three samples are 62 kPa, 64 kPa and 65 kPa. These values represent an over-consolidation ratio (OCR) of 7, 3 and 1.5 for the three tested samples and from top to bottom respectively. Considering the sedimentation history in the area the shallow high OCRs are probably apparent and the sediments are most likely normally consolidated. Table 2 shows the most important parameters derived from the consolidation tests.

a)

	e	W_i (%)	W_P (%)	W_L (%)	C_c	k (m^2)	s (m^{-1})	σ_c (kPa)
SVAIS-02-02	1.83	44.2	22.0	44.3	0.59	$2.3 \cdot 10^{-14}$	0.024	62
SVAIS-02-04	1.75	39.0	19.2	47.1	0.36	$6.2 \cdot 10^{-16}$	0.025	64
SVAIS-02-06	0.91	23.1	15.0	31.5	0.19	$5.9 \cdot 10^{-17}$	0.015	65

Table 2: Most important parameters derived from this study. e: initial void ratio, W_i: initial water content, W_P: plastic limit, W_L: liquid limit, C_c: Consolidation coefficient, s: initial specific storage, σ_c: pre-consolidation pressure.

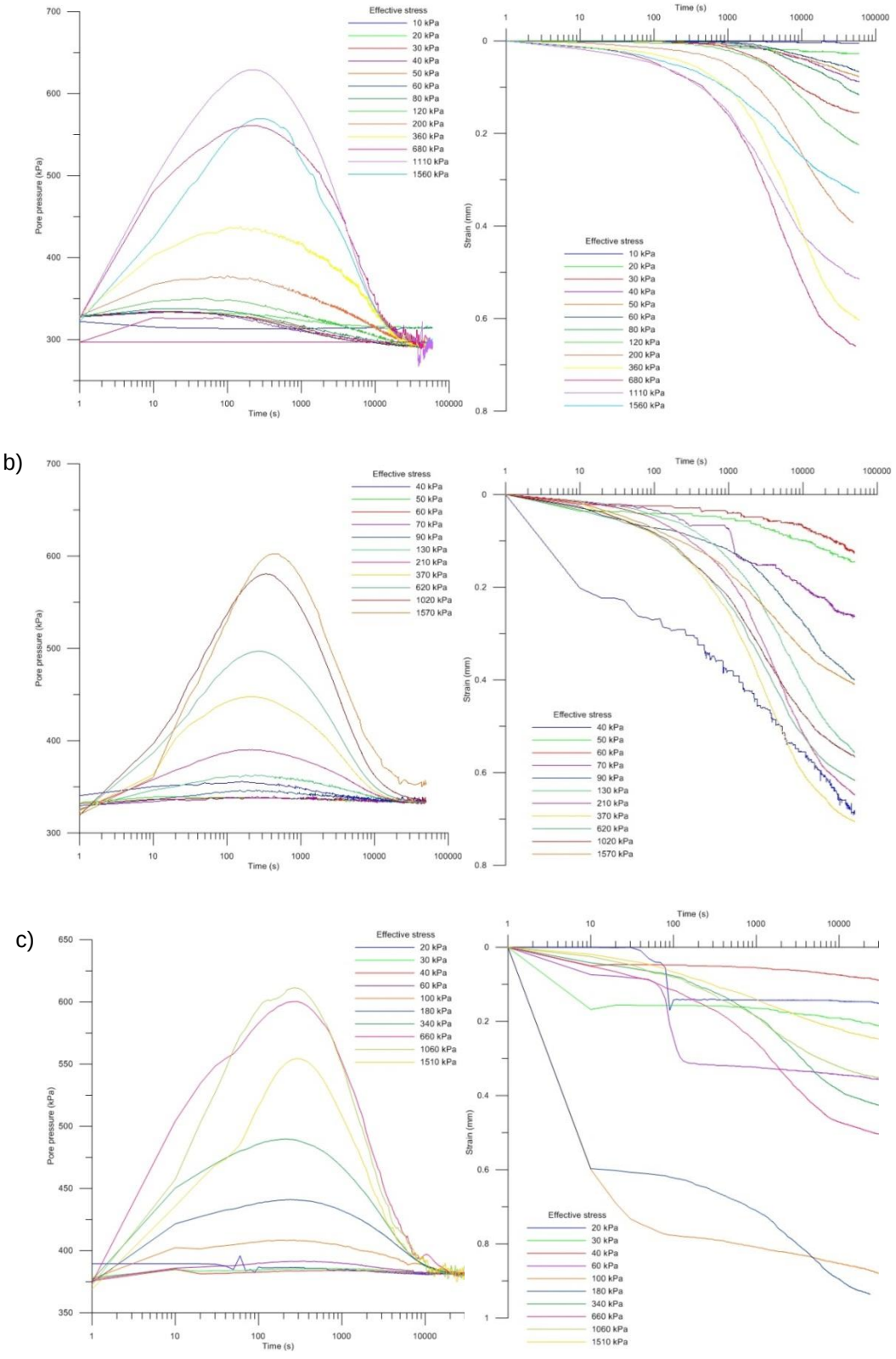

Fig. 6 Pore pressure and strain during consolidation. a) SVAIS-02-02, b) SVAIS-02-04 and c) SVAIS-02-06.

The samples tested have shown that turbidites have higher initial hydraulic conductivity (1.2 x 10^{-7} m/s compared to 5.9 x 10^{-10} m/s) and compressibility

(0.35 versus 0.19 than glacial debris flows. The specific storage and permeabilities determined for each consolidation stage and for each sample show also higher decrease with increasing stress for turbidite sediments than the GDF's (Table 2 and Fig. 8).

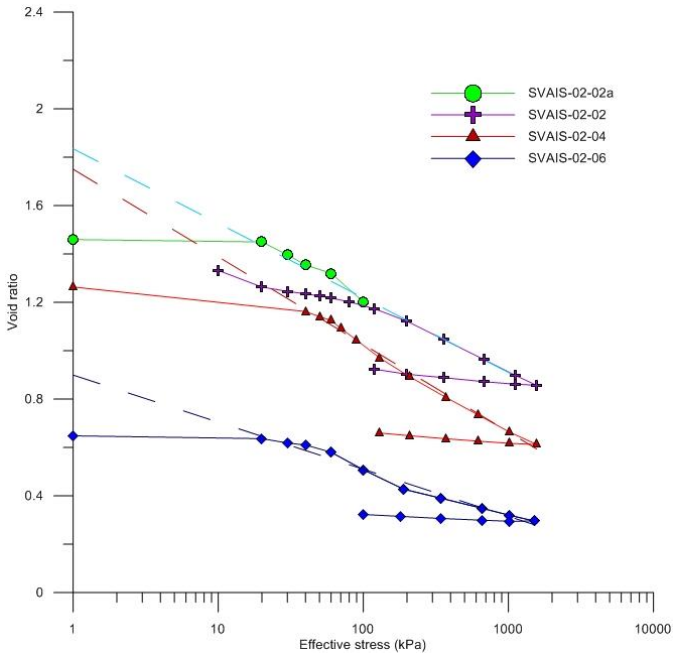

Fig. 7 Consolidation tests: effective stress/void ratio relationship for the tested samples.

The consolidation coefficients obtained from the consolidation test are 0.59 and 0.36 for samples SVAIS02-02 and SVAIS02-04. Because the very little definition in the slope of the virgin consolidation line, we provide a range of between 0.25 and 0.15, with a mean value of 0.19 for the consolidation coefficient of sample SVAIS-02-06.

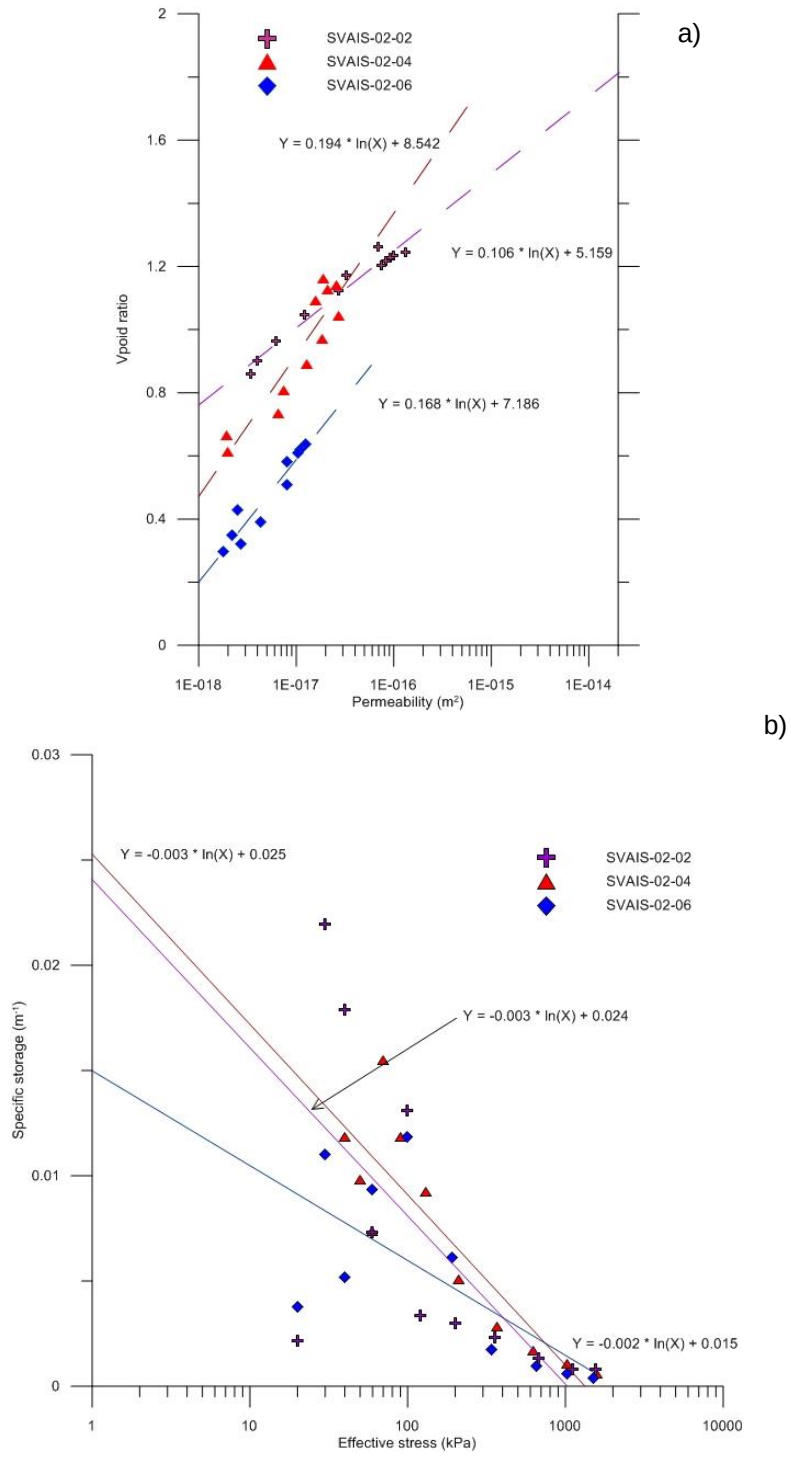

Fig. 8 a) Permeability versus void ratio for each sample. Initial permeability results from intersection of the theoretical permeability curves with the initial void ratio determined. b) Effective stress versus specific storage for each sample. Extrapolation to 1 kPa is used to determine initial parameters for the simulation

The consolidation test provides various input parameters that can be used in "BASIN" modelling. These parameters include initial porosity, hydraulic conductivity and specific storage (see Table 3). As mentioned above "BASIN"

allows four sediment types. In this study, the sediment types were defined as turbidites (including plumites), GDF's, tills and hemipelagic sediments. However, consolidation tests were only performed in turbidites and GDF's. Parameters for tills and hemipelagic sediments are taken from the literature (Table 3). The total length of the modelled transect is around 162 km and the mesh nodes are equally spaced every 4 km. Given the model limitations, ice-induced stresses or erosion by ice have not been considered. Sedimentary facies are not only composed of one unique sediment type, but often they are a mixture of the sediment types described above. The composition of the mixture will vary according to the relative abundance of each sediment type for a given area and unit defined. Generally the continental shelf is composed mainly by tills and a little portion of turbidites. The slope is a mixture of turbidites, hemipelagic sediments (~40%) and debris flows (~60%). The lower slope and abyssal plain are mainly composed by turbidites and hemipelagic sediments, with the content of the latter type of sediment increasing towards the distal part of the model.

	Turbidites	GDF's	Till	Hemipelagic sediments
Initial porosity	0.63 [(1)]	0.47 [(1)]	0.4 [(5)]	0.75 [(3)]
Grain density (kg/m^3)	2650	2650	2650	2650
Initial Specific storage (m^{-1})	0.025 [(1)]	0.015 [(1)]	0.0056 [(2)]	0.04 [(4)]
Init. hydraulic conductivity (m/s)	1.2 x 10^{-7} [(1)]	5.9 x 10^{-10} [(1)]	5.3 x 10^{-11} [(5)]	3.0 x 10^{-9} [(4)]

Table 3 Parameters used for "BASIN" and fluid flow modelling. [(1)] this study. [(2)] Shaver, 1998. [(3)] Butt et al. 2000. [(4)] Urgeles et al. 2010. [(5)] Solheim et al. 1991.

Sedimentation modelling was subdivided in 33 sub-steps. Each sub-step is defined by a sediment thickness along the model, sediment composition and time interval. Time intervals were extracted from Hjelstuen et al., 2007 (Fig 4c).

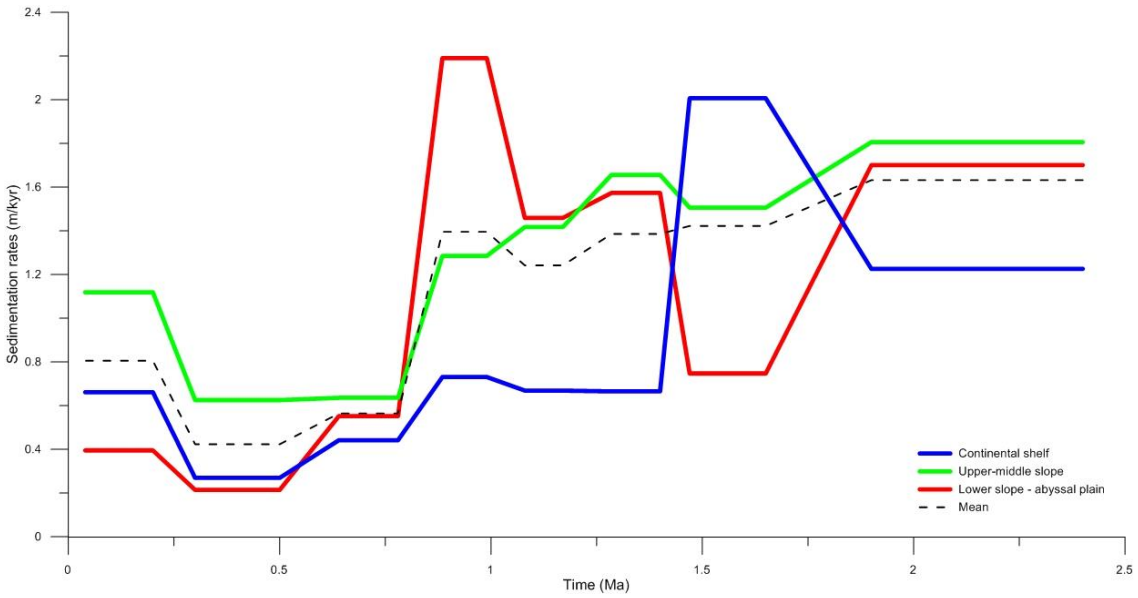

Fig 9 Sedimentation rates for every sub-step in "BASIN" hydrogeological modelling (stages between oceanic basement and reflector R7 no shown).

According with the values derived from the seismic reflection data the mean sedimentation rate is around 1.1 m/kyr with maximum values of 2.5 m/kyr (Fig. 9). These values are in agreement with those proposed by Pedrosa et al. (2011), for the Holocene and Last Glacial Maximum, and Hjelstuen et al. (1996). Fig. 9 shows the sedimentation rates for every sub-step in between reflectors R7 and the seafloor used as input for the model.

The program "BASIN" allows to generate multiple output graphic results. The results of the simulation at the final stage (present) are shown in Fig. 10. The main physical properties and sedimentological/architectural characteristics considered here are presented. At the end of the simulation, the minimum porosities are around 10 %, mainly corresponding to the units made of tills and glacigenic debris flows. Hydraulic conductivities for these units have values between 10^{-12} and 10^{-10} m/s. Pore pressures reach values of 6700 kPa at the vertical of the shelf break where the sediment thickness is maximum. When the pore pressures are converted in overpressure the results show maximum values of ~0.7. These occur in the area where hydraulic conductivity is lower associated with deposition of a higher amount of till sediments between R5 and R2 reflectors.

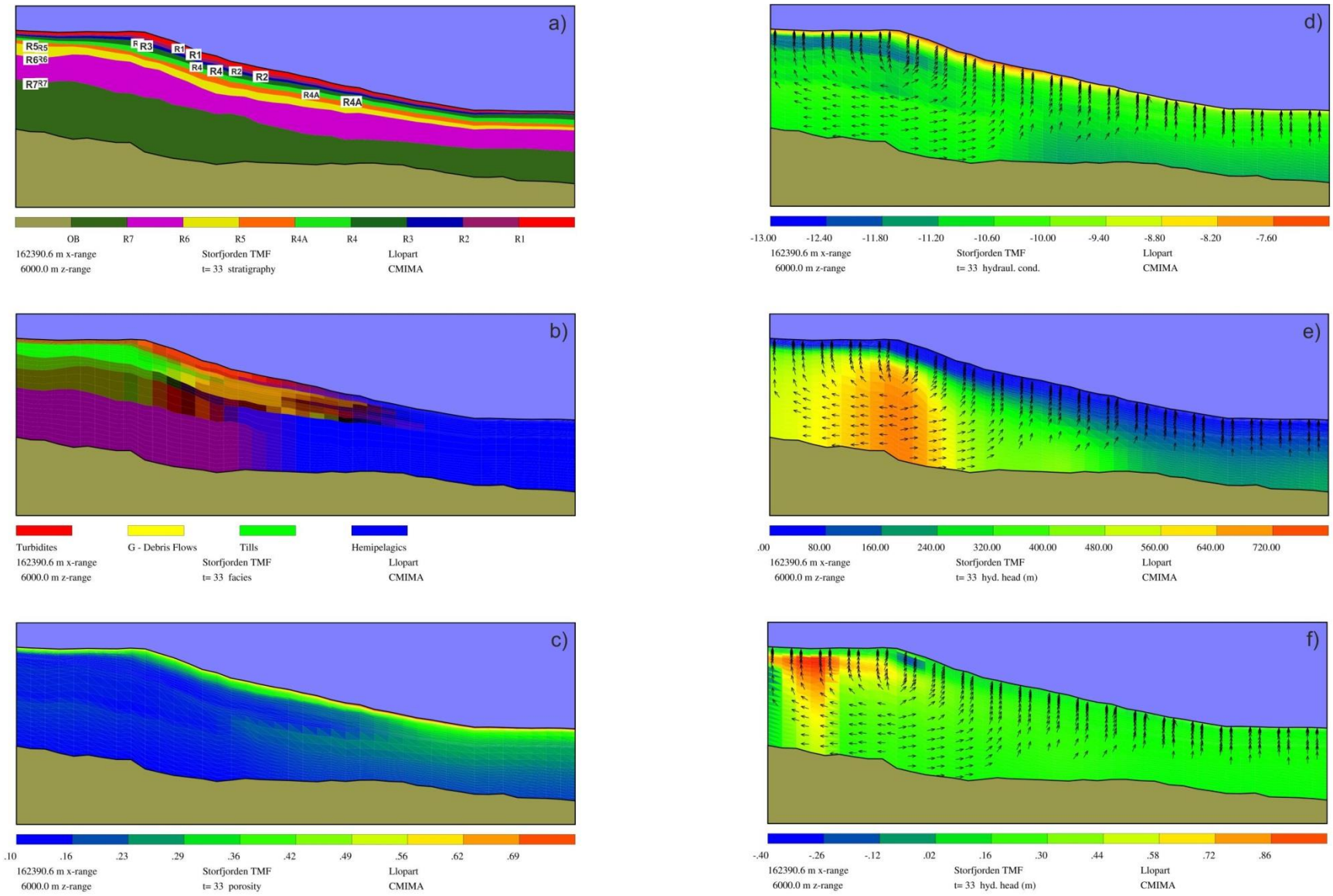

Fig 10 Margin stratigraphic and hydrodinamic modelling with “BASIN”at final simulated present condition. (a) Margin stratigraphy according to seismic units described for Faleide et al. 1996. (b) Facies composition. (c) Fractional porosity. (d) Log hydraulic conductivity. (e) Excess pore pressure. (f) Overpressure (λ).

5. Discussion

The consolidation tests performed in this study clearly show that climatically controlled sedimentation changes on glaciated continental margins, produces sediments with contracting physical properties. In this case, samples SVAIS-02-02, SVAIS-02-04 corresponding to melt water hyperpycnal flows or turbidites (plumites), which were taken from the upper part of the core, have high hydraulic conductivity, high porosity and high consolidation index compared to sample SVAIS-02-06, which was taken on glacigenic debris flows sediments. These differences are partially controlled by consolidation, but trends in the virgin consolidation line and theoretical permeability indicate that the differences are genuine (Figs. 7 and 8a). According to the tests performed on core SVAIS-02 when it was splitted, turbidites also have higher water content and lower shear strength than the GDF's. Turbidites are finer grained and better sorted than GDF's which is probably at the origin of the observed differences in physical properties.

"BASIN" modelling allows us to understand how physical properties, sedimentology and stratigraphic architecture couple to control margin hydrogeology and fluid flow pathways. It should be noted, however, that the seafloor depth at the final stage of the model, does not perfectly match that observed in the data and this may result from the input parameters used for tills and hemipelagic sediments obtained from the literature.

The simulation shows that low porosities (10%-25%) develop in most of the continental margin, specially the continental shelf and upper-middle slope, due to consolidation. Porosity reaches values of 10% at 125 mbsf in the continental shelf zone and at 250-280 mbsf at the shelf break and upper-middle slope (Fig. 11). Porosity values of ODP Site 986 (Fig 11) are slightly higher than model porosity. According to Bear (1972), the hydraulic conductivity values of sediments with such a low porosity corresponds with that of impervious materials ($K<10^{-6}$). The model shows that hydraulic conductivity in the upper part of the continental shelf package is low between reflectors R5-R2. This

interval has a higher content in till and glacigenic debris flow type sedimentation, which originally has a lower initial hydraulic conductivity (Table 3). This fact is responsible for a higher hydraulic conductivity layer at the bottom of the sedimentary succession. Around the shelf break the mean sedimentation rates are higher due to margin progradation resulting in excess pore pressure build-up (high hydraulic head) which results in fluid flow divergence (Fig. 10e).

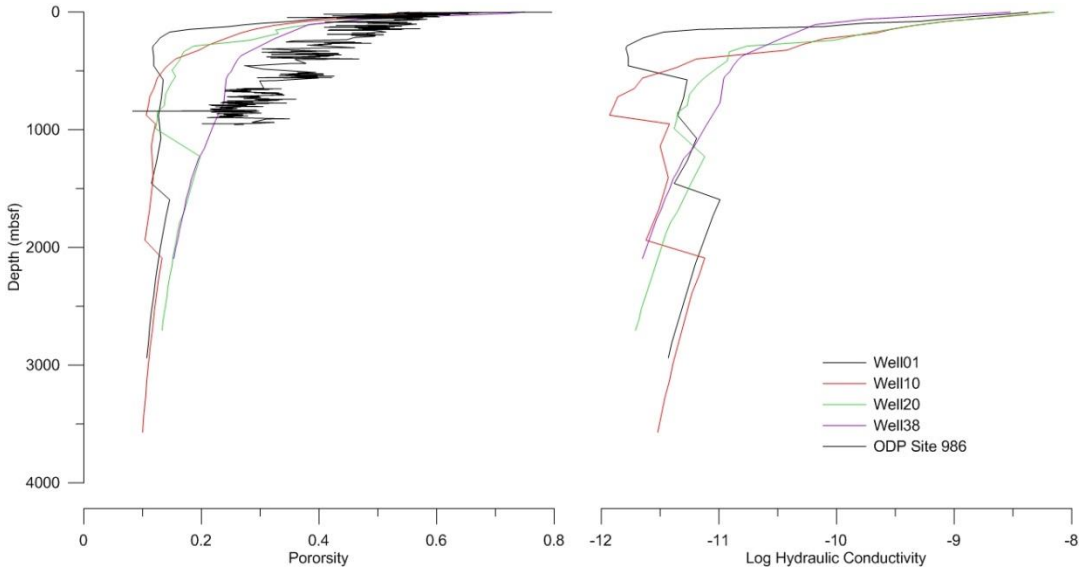

Fig 11 Present day values for porosity and hydraulic conductivity at nodes (wells) 1, 10, 20 and 38 of the simulation mesh. These nodes correspond to left boundary of the model, shelf break middle slope and distal zone, respectively. Also shown are the porosities at ODP Site 986 for comparison with the modeled porosities at the distalmost model well (38).

Despite the fluid flow divergence determines the flow pattern, most of the margin shows vertical fluid flow which is a normal situation for a fluid flow trend in a continental margin dominated by consolidation processes. The high sedimentation rates between 2.4-1.65 Ma B.P. in the continental slope and between 1.65 B.P. and 1.4 Ma B.P. in the continental shelf, together with predominance of till and glacigenic debris flows sedimentation between reflectors R5-R2 in these two areas is responsible for the development of the modeled excess pore pressure close to the shelf break. The low permeability of glacial sediments imposes an upper low hydraulic conductivity boundary that enhances pore pressure build-up. Further to this, the boundary conditions imposed by the model (left impervious boundary) additionally contribute to the development of excess pore pressure. This fact causes instabilities in the

lambda simulation resulting in wrong values of overpressure. The sensitivity analysis carried out with the model shows that at modelled sedimentation rates between reflectors R7-R6 the model becomes unstable; with lower sedimentation rates the model remains stable.

The maximum values of overpressure (see equation 10) are ~0.43 below the shelf break. Overpressure values over 0.25 appear at 0.99-0.89 Ma B.P. and gradually increase to 0.7 at 0.7 Ma B.P., and these values have been kept without important variations to present day. Despite the instability of the nodes on the easternmost side of the model, a zone of high overpressure enclosed between 150-800 mbsf is still visible near the left boundary of the model and particularly between 550-1500 mbsf at the shelf break. These depths correspond to the region in which the pore pressure curve is proportionally closer to the lithostatic stress (Fig 12).

The areas of higher overpressure (Fig. 10f) where the slope gradient is also larger (continental slope) are the places where slope instability is more likely to take place. The Hinlopen Slide is an example of deep seated failure rooted at depths exceeding 1400 mbsf (Vanneste et al., 2006). Pedrosa et al. (2011) also identified submarine landslides rooted at depths between 500-1000 m in the Storfjorden area, thus observed failures are compatible with modeled overpressures.

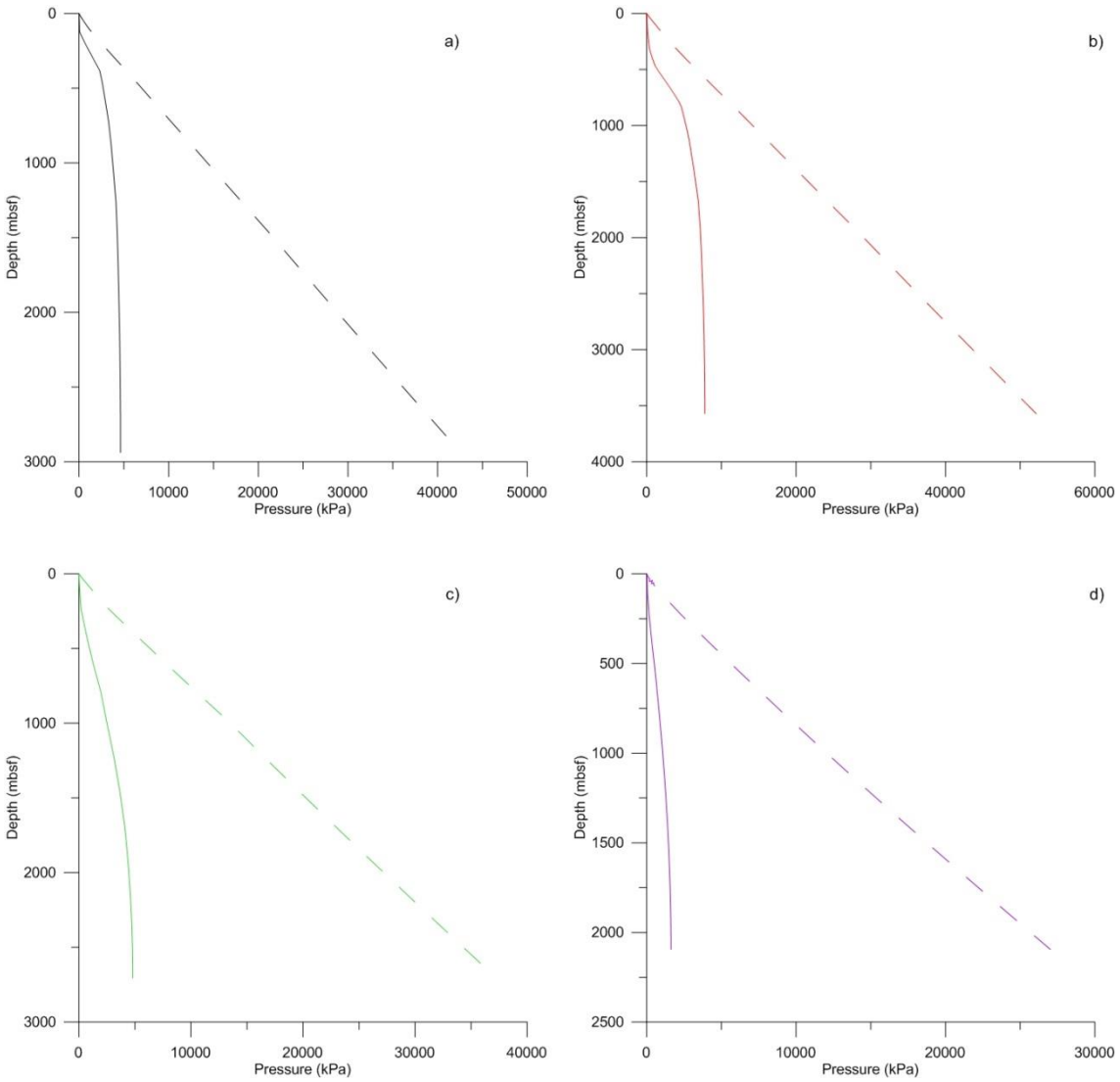

Fig 12 Solid line shows present day values for excess pore pressure (above hydrostatic). Dashed line shows hydrostatic effective stress. a) node 1, b) node 10, c) node 20 and d) node 38. These nodes correspond to left boundary of the model, shelf break, middle slope and distal zone, respectively.

6. Conclusions

Consolidation tests have been carried out to determine the compressibility and permeability characteristics of glacial and glacially influenced sediments of the upper slope of the Storfjorden TMF, western Barents Sea. Three samples, SVAIS-02-02, SVAIS-02-04 and SVAIS-02-06 were tested. The first two correspond to turbidite-like sediments and the third is made of GDF's. The main results of the laboratory testing program show that turbidites (glacial melt-water plumites; samples SVAIS-02-02, SVAIS-02-04) have high void ratios, consolidation coefficients and permeabilities with respect to glacigenic debris flows (sample) at initial deposition conditions. The respective values for all samples are the following:

- Void ratios are 1.83 for SVAIS-02-02, 1.75 for SVAIS-02-04 and 0.91 for SVAIS-02-06.
- Consolidation coefficients are 0.59 for SVAIS-02-02, 0.36 for SVAIS-02-04 and 0.19 for SVAIS-02-06.
- Permeabilities are $2.3 \cdot 10^{-14}$ for SVAIS-02-02, $6.2 \cdot 10^{-16}$ for SVAIS-02-04 and $5.9 \cdot 10^{-17}$ for SVAIS-02-06.

All samples have a similar pre-consolidation pressure of between 62-65 kPa. These values of pre-consolidation pressure represent an OCR of 7, 3 and 1.5, for the three samples respectively, which is interpreted as apparent in this study.

The compressibility and permeability values, together with stratigraphic input from seismic reflection profiles, were used in "BASIN" modelling to understand the influence of glacial continental margin sedimentation in fluid flow patterns. Modelling included four main sediment types: turbidites, GDFs, tills and hemipelagic sediments. Values of till and hemipelagic sediments were taken from the literature and ODP site 986 results. The latest stage of the model (present day) shows low porosities and hydraulic conductivities between reflectors R5-R1 in the continental shelf zone. The higher sedimentation rates around the shelf break due to progradation are responsible for fluid flow

divergence, which affects the entire fluid flow pattern of the continental margin. The lower hydraulic conductivity of glacial sediments, particularly when compressed, combined with flow divergence causes model instabilities. Despite this, overpressure clearly shows that lower effective stresses develop at the outer continental shelf and the shelf break at 550-1500 mbsf indicating a likely pre-conditioning for deep-seated failure.

7. Acknowledgements

This study is part of the research project funded by the "Ministerio de Ciencia e Innovación" through grants DEGLABAR (CTM2010-17386) and SVAIS (POL2006-07390). UNESCO and IUGS are also acknowledged for networking funding through project IGCP-585. The ‘‘Generalitat de Catalunya’’ is acknowledged for support through an excellence research group grant (2009-SGR-146). Funding through ACI2009-1037 is also acknowledged. Institute of Marine Sciences of CSIC provided the scientific and laboratory infrastructures necessary to develop the experimental tests. Moreover, I would like to acknowledge Dr. Roger Urgeles, and Dr. Angelo Camerlenghi for their patience, knowledge that they have contributed and the comments and ideas provided. Mayte Pedrosa is also acknowledged for providing the seismic reflectors used for input to modeling.

8. References

Andreassen, K., Nilssen, L.C., Rafaelsen, B., Kuilman, L., 2004. Three-dimensional seismic data from the Barents Sea margin reveal evidence of past ice streams and their dynamics. Geology, 32, 729–732.

Bear, J., 1972. Dynamics of Fluids in Porous Media. American Elsevier Publications Co.

Bitzer, K., 1999. Two-dimensional simulation of clastic and carbonate sedimentation, consolidation, subsidence, fluid flow, heat flow and solute transport during the formation of sedimentary basins. Computers & Geosciences, 25(4), 431-447.

Bitzer, K., 1996. Modelling consolidation and fluid flow in sedimentary basins. Computers & Geosciences, 22 (5), 467-478.

British Standards Institution, 1990. British standards methods for soil civil engineering purposes. Part 6.

Bugge, T., Belderson, R.H. and Kenyon, N.H., 1988. The Storegga Slide. Philosophical Transactions of the Royal Society of London, 325, 357-388.

Bugge, T., Befring, S., Belderson, R.H., Eidvin, T., Jansen, E., Kenyon, N.H., Holtedahl, H. and Sejrup, H.P., 1987. A giant three-stage submarine slide off Norway. Geo-Marine Letters, 7, 191-198.

Bugge, T., 1983. Submarine Slides on the Norwegian Continental Margin, with Special Emphasis on the Storegga Area. Continental Shelf and Petroleum Research Institute Publication, 110, 152 pp. Trondheim, Norway.

Butt, F.A., Drange, H., Elverhø, A., Otterå, O.H. and Solheim, A., 2002. Modelling Late Cenozoic isostatic elevation changes in the Barents Sea and their implication for oceanic and climatic regimes: preliminary results. Quaternary Science. Review, 21, 1643-1660.

Butt, F.A., Elverhøi, A., Solheim, A., F. C. F., 2000. Deciphering Late Cenozoic development of the western Svalbard Margin from ODP Site 986 results. Marine Geology, 169(3-4), 373-390.

Dahlgren, K.I.T., Vorren, T.O., Stoker, M.S., Nielsen, T., Nygård, A. and Sejrup, H.P., 2005. Late Cenozoic prograding wedges on the NW European continental margin: their formation and relationship to tectonics and climate. Marine and Petroleum Geology, 22, 9-10.

Dimakis, P., Elverhøi, A., Hoeg, K., Solheim, A., Harbitz, C., Laberg, J. S., Vorren, T. O. and Marr, J., 2000. Submarine slope stability on high-latitude glaciated Svalbard–Barents Sea margin. Marine Geology, 162, 303-316.

Elverhøi, A., Dowdeswell, J., Funder, S., Mangerud, J. and Stein, R., 1998. Glacial and oceanic history of the Polar North Atlantic margins: an overview. Quaternary Science Review, 17, 1-3.

Elverhøi, A., Fjeldskaar, W., Solheim, A., Nyland-Berg, M., Russwurm, L., 1993. The Barents Sea Ice Sheet - A model of its growth and decay during the last ice maximum. Science, 12, 863-873.

Engen, Ø., Faleide, J. and Dyreng, T., 2008. Opening of the Fram Starit gateway: A review of plate tectonic constrains. Tecthonophysics, 450, 51-69.

Faleide, J., Solheim, A., Fiedler, A., Hjelstuen, B., Andersen, E. and Vanneste, K., 1996. Late Cenozoic evolution of the western Barents Sea-Svalbard continental margin. Global and Planetary Change, 12, 53-74.

Fiedler, A. and Faleide, J.I., 1996. Cenozoic sedimentation along the southwestern Barents Sea margin in relation to uplift and erosion of the shelf. Global Planet. Change, 12, 75–94.

Forsberg, C.F., Solheim, A., Elverhøi, A., Jansen, E., Channell, J.E.T., 1999. The depositional environment of the western Svalbard margin during the Pliocene and the Pleistocene: Sedimentary facies changes at Site 986. Proceedings of the Ocean Drilling Program, Scientific Results 162, 233–246.

Hjelstuen, B.O, Eldholm, O., Faleide, J.I., 2007. Recurrent Pleistocene mega-faliures on the SW Barents Sea margin. Earths and Planetary Science Letters, 258, 605-618.

Hjelstuen, B.O, Elverhøi, A., Faleide, J.I, 1996. Cenozoic erosion and sedimentary yield in the dranaige area of the Storfjorden Fan. Global and Planetary Change,12, 95-116.

Karlsson, R., 1961. Suggesting improvements in the liquid limits test, with reference to flow properties of remolded clays. 5th Conference On Soil Mechanics and Foundations Engineering, 1, 171.

Knies, J., Matthiessen, J., Vogt, C., Laberg, J.S., Hjelstuen, B.O., Smelror, M., Larsen, E., Andreassen, K., Eidvin, T. and Vorren, T.O., 2009. The Plio-Pleistocene glaciation of the Barents Sea–Svalbard region: a new model based on revised chronostratigraphy. Quaternary Science Reviews, 28, 812-829.

Kuvaas, B. and Kristoffersen, Y., 1996. Mass movements in glaciomarine sediments on the Bares Sea continental slope. Global Planet. Change, 12, 287–308.

Laberg, J.S. and Vorren, T.O., 1996a. The middle and late Pleistocene evolution of the Bear Island Trough Mouth Fan. Global Planet. Change 12, 309–330.

Laberg, J.S. and Vorren, T.O., 1996b. The glacier-fed fan at the mouth of Storfjorden trough, western Barents Sea: a comparative study. Geology. Rundsch, 85, 338–349.

Lucchi, R.G., Pedrosa, M.T., Camerlenghi, A., Urgeles, R., De Mol, B., Rebesco, M., 2012. Recent submarine landslides on the continental slope of Storfjorden and Kveithola Trough-Mouth Fans (north west Barents Sea). In Yamada, Y., Kawamura, K., Ikehara, K., Ogawa, Y., Urgeles, R., Mosher, D., Chaytor, J. and Strasser, M. (Eds.) Submarine Mass Movement and Their Consequences, Advances in Natural and Technological Hazards Research, 34, Springer, Dordrecht (The Netherlands), in press.

Mulder, T. and Moran, K., 1995. Relationship among submarine instabilities, sea level variations, and the presence of an ice sheet on the continental shelf: An example from the Verrill Canyon area, Scotian shelf. Paleoceanography, 10, 137-154.

Pedrosa, M.T., Camerlenghi, A., De Mol, B., Urgeles, R., Rebesco, M., Lucchi, R.G. and shipboard participants of the SVAIS and EGLACOM Cruises, 2011. Seabed morphology and shallow sedimentary structure of the Storfjorden and Kveithola trough-mouth fans (North West Barents Sea). Marine Geology, 286, 65-81.

Sættem, J., Poole, D.A.R., Sejrup, H.P. and Ellingsen, K.L., 1992. Glacial geology of outer Bjornoyrenna, southwestern Barents Sea. Marine Geology, 103, 15-51.

Shaver, R., 1998. The determination of glacial till specific storage in North Dakota. Ground Water, 36, 4, 552-557.

Solheim, A., Faleide, J., Andersen, E., Elverhøi, A. and Fiedler, A., 1998. Late Cenozoic seismic stratigraphy and glacial geological development of the east Greenland and Svalbard-Barents Sea continental margins. Quaternary Science Reviews, 17, 155-184.

Solheim, A., Forsberg, C. F. and Pittenger, A., 1991. Geotechnical properties of glacigenic shelf sediments from Prydz Bay, East Antarctica. Proceedings of the Ocean Drilling Program, Scientific Results, 119, 143-167.

Sultan, N., Cochonat, P., Foucher, J.-P. and Mienert, J., 2004. Effect of gas hydrates melting on seafloor slope instability, Marine Geology, 213, 379-401.

Urgeles, R., Locat, J., Sawyer, D.E., Flemings, P.B., Dugan, B. and Binh, N.T.T., 2010. History of pore pressure build up and slope instability in mud-dominated sediments of Ursa basin, Gulf of Mexico continental slope. In Submarine mass movements and their consequences, advances in natural and technological hazards research, eds. Mosher D.C., Moscardelli, L., Shipp, R.C., Chaytor, J.D., Baxter, C.D.P., Lee, H.J., Urgeles, R. Springer, 28, 179-190.

van Hinte, J.E., 1978. Geohistory analysis-application of micropaleontology in exploration geology. Am. Assoc. Pet. Geol. Bull., 62, 201–222

Vanneste, M., Mienert, J. and Bunz, S., 2006. The Hinlopen Slide: A giant, submarine slope failure on the northern Svalbard margin, Arctic Ocean. Earth and Planetary Science Letters, 245, 373-388.

Vorren, T.O., Lebesbye, E. and Larsen, K., 1990. Geometry and genesis of the glacigenic sediments in the southern Barents Sea. In Glacimarine Environments: Processes and Sediments, eds. Dowdeswell J.A. and Scource J.D. Geological Society Special Publication, 53, 309-328.

Vorren, T., Laberg, J., Blaume, F., Dowdeswell, J., Kenyon, N., Mienert, J., Rumohr, J.,Werner, F.,1998. The Norwegian-Greenland Sea continental margins: morphology and late Quaternary sedimentary processes and environment. Quaternary Science Reviews, 17, 273-302.